ELSEVIER

Earth and Planetary Science Letters 203 (2002) 519–534

EPSL

www.elsevier.com/locate/epsl

Long-range detection of hydroacoustic signals from large icebergs in the Ross Sea, Antarctica

Jacques Talandier [a], Olivier Hyvernaud [b], Emile A. Okal [c,*], Pierre-Franck Piserchia [a]

[a] *Département Analyse et Surveillance de l'Environnement, Commissariat à l'Energie Atomique, B.P. 12, F-91680 Bruyères-le-Châtel, France*

[b] *Laboratoire de Détection et Géophysique, Commissariat à l'Energie Atomique, B.P. 640, F-98713 Papeete, Tahiti, French Polynesia*

[c] *Department of Geological Sciences, Northwestern University, Evanston, IL 60208, USA*

Abstract

Hydroacoustic signals detected in late 2000 by seismic stations in Polynesia are shown to originate from huge icebergs which at the time were drifting in the Ross Sea after calving off the Ross Ice Shelf. The signals present a broad variety of spectral characteristics, most of them featuring prominent eigenfrequencies in the 4–7 Hz range, often complemented by overtones. Most epicenters, obtained by combining observations of distant hydroacoustic and regional seismic records, follow the spatio–temporal evolution of the drift of iceberg B-15B. Most of the signals are generated during a 36-day time window when it is speculated that B-15B collided with smaller icebergs or was scraping the ocean floor on the shallow continental shelf. We speculate on the possible physical nature of the resonator generating the signals, which could correspond to an elastic mode of the iceberg, or to the oscillation of fluid-filled cracks in the ice.

Keywords: acoustical methods; seismic waves; icebergs

1. Introduction

We report in this paper the detection by the Polynesian Seismic Network (Réseau Sismique Polynésien; hereafter RSP) of hydroacoustic signals (T phases) originating from huge icebergs which were drifting in the Ross Sea in Late 2000, after calving off the Ross Ice Shelf around May 2000. The signals offer a broad variety of spectral characteristics and the exact nature of their sources remains speculative. However, their locations, obtained from a combination of distant T phases and of seismic waves recorded at land-based Antarctic stations, correlate perfectly with the positions of the bergs, as tracked by satellite imagery, thus clearly associating the acoustic sources with mechanical processes inside the icebergs. In the context of the monitoring of the Comprehensive Nuclear-Test Ban Treaty (CTBT), these events provide new insight into the nature of sources contributing energy into the hydroacoustic spectrum. They further illustrate the powerful synergy achieved by combining datasets of a different nature, i.e. regional seismic waves and T phases recorded at island stations.

* Corresponding author. Tel.: +1-847-491-3238; Fax: +1-847-491-8060.
E-mail address: emile@earth.nwu.edu (E.A. Okal).

0012-821X/02/$ – see front matter
PII: S0012-821X(02)00867-1

The RSP has been described in many previous publications [1]. The operation, at its sites, of recording channels equipped with filters boosting magnification in the 2–10 Hz range [2] helped introduce the concept of the T-phase stations later mandated by the CTBT [3]. The detection capabilities of the RSP were highlighted during the Hollister swarm of 1991–1993, leading Talandier and Okal [4] to the identification of a major volcanic edifice linking the Pacific–Antarctic Ridge to the Louisville Ridge, later discovered and surveyed by Géli et al. [5], during a cruise of the N/O *L'Atalante*.

2. Detection

2.1. General characteristics of the signals

Starting in August 2000, the RSP stations at Tubuai (TBI), Vaihoa (VAH), Taravao (TVO), and Rikitea (RKT) detected irregular activity originating from the Southern Ocean. We report here on a group of 13 sequences (hereafter the 'Ross Events') with most of the activity concentrated in November and December 2000. Their principal properties are listed in Table 1, and Fig. 1A–D shows representative spectrograms of signals recorded at VAH, a station located on the southern shore of the atoll of Rangiroa. In such conditions, the acoustic-to-seismic conversion is particularly efficient [6], and given the short post-conversion path (not exceeding 100 m), the seismic signal at the T-phase station is essentially equivalent to the acoustic one inside the SOFAR, within the frequency window of interest ($2 \leq f \leq 16$ Hz). The examples shown document a remarkable variability among events. In most instances, the energy is concentrated at one or several prominent frequencies, which suggests that its source must involve the oscillation of some kind of resonator, a model also supported by the often long duration of the signals, e.g. Event 4, which lasted for 3 h. However, some sequences feature significantly broader spectra (e.g. Event 12), and some, like Event 2 (Fig. 1A), last no more than 2 min. In addition, the frequency of the largely monochromatic signals does fluctuate with time, a property already observed during the Hollister swarm [4], with some of the Ross events featuring more substantial variations of frequency with time (e.g. Event 7, see below, Section 4), which give the spectrograms a contorted, 'snake-shaped' aspect. Finally, several sequences end with singular signals exhibiting an increase of frequency with time (suggestive of the shrinking of the resonator), which can be slow and gradual (Event 4) or fast and abrupt (Event 3, Fig. 1B). Event 13 (Fig. 1D) terminates through a complex evolution of prominent frequencies with time, featuring several episodes of frequency decrease, a property termed 'gliding' and identified during episodes of volcanic tremor [7], which in general terms would suggest a geometrical expansion of the resonator [8].

2.2. Detection of T phases at other sites

A systematic effort was made to complement the RSP dataset with records at other Pacific seismic stations (Fig. 2). When available, the IRIS station at Rarotonga (RAR) provided increased azimuthal aperture; it was, however, inoperative from 04 to 18 December 2000. Unfortunately, no other seismic station could contribute T-phase signals, and this for a variety of reasons, which we deem important to discuss, as they give insight into the performance of seismic stations as hydroacoustic detectors, notably in the context of the monitoring of the CTBT. These include blockage (by the large Campbell Plateau and New Zealand) at Noumea (NOUC), by the Samoa Islands at Johnston (JOHN), and by Rangiroa and the Tuamotu Plateau at the ocean-bottom observatory H2O, where neither a seismic nor a pressure signal could be detected; unfavorable station locations involving long post-conversion seismic paths at Tasmania University (TAU), Kipapa (KIP) and Christmas (XMAS); a probable combination of those two effects at Van Inlet (VIB), blocked by the Tuamotu Plateau east of VAH (Fig. 2B); and a high level of background noise at the small island of Pitcairn (PTCN). Finally, no signal was identified at Easter Island (RPN), where T-phase detection has been previously recognized as irregular [9–11]. In this respect, and despite the gener-

Table 1
Principal characteristics of the 13 events studied

Number	Date and time	Epicenter		Duration	Peak-to-peak velocity at VAH	Remarks
	D M (J)	(°S)	(°E)	(min)	(μm/s)	
1	15 AUG (228) 22:28:18.6	78.21	−168.61	1.3	1.23	Edge of Ross Ice Shelf. No data at RAR, RKT. Monochromatic signal (3.5 Hz) with overtones; sharp impulsive beginning.
2	08 NOV (313) 22:18:31.3	72.10	170.16	2	2.18	Borchgrevink Land. Relatively monochromatic; frequency fluctuates; no overtones.
3	12 NOV (317) 01:13:26.6	75.76	−175.75	8	0.62	Central Ross Sea. Generally weak at Antarctic stations. Narrow spectrum centered around 4 Hz. Strong final puff with frequency increasing with time.
4	12 NOV (317) 06:00–09:00	75.8	−175.8	3 h	0.24	Central Ross Sea. Only traces in Polynesia (except VAH); no signal at SBA and Erebus. Long signal, generally monochromatic (2.5–4 Hz), with frequency fluctuations but few overtones.
5	14 NOV (319) 01:01:56.6	75.92	−175.60	3	0.81	Central Ross Sea. No data: Erebus; no signal: SBA. Relatively broad spectrum on acoustic records. Dominant frequency 2.5 Hz at VNDA.
6	19 NOV (324) ≈02:30	75.8	−175.8	10	0.42	No signal: RSP except VAH. No data: Erebus, SBA. Broad spectrum (2–16 Hz). Assumed in same area as Events 3–5, based on times at VNDA and VAH.
7	21 NOV (326) 15:22	75.8	−175.8	10	0.24	No signal: Polynesia except VAH. No data: Erebus, SBA. Fluctuation of dominant *f*, leading to 'snake-shaped' spectrogram. Assumed at same location as Events 4–6, based on VNDA and VAH times.
8	22 NOV (327) 21:32:13.0	75.85	−176.28	10	0.34	Central Ross Sea. No data: Erebus, SBA. Same general characteristics as Event 7.
9	05 DEC (340) 03:21:19.8	75.08	−177.75	8	0.30	Central Ross Sea. No data: Erebus; no signal: SBA. Broad spectrum (2–10 Hz), with dominant $f = 2.9$ Hz. Final sequence with sharply increasing frequency.
10	05 DEC (340) ≈20:46	75.1	−177.8	15	0.32	Noisy record; broad spectrum (2–10 Hz), with two sequences; assumed to share location of Event 9.
11	15 DEC (350) 03:16:14	74.4	−178.4	10	0.44	Central Ross Sea. No signal: SBA. Broad spectra (2–12 Hz); weak correlation of acoustic and seismic records.
12	18 DEC (353) 09:56:29.1	74.82	−178.68	8	0.42	Central Ross Sea. Two parts; first short (30 s) with impulsive start; second emergent and long (150 s). Broad spectrum.
13	14 JAN (014) 2001 17:36:10	67.0	141.5	7	1.31	Off Oates or George V coasts. No signal: RKT; all Antarctic stations. Relatively broad spectrum with dominant *f* at 4, 5.5 and 7 Hz; first sequence ends abruptly, followed by short (60 s) puff, with spectrogram showing several lines of strongly decreasing frequencies (gliding). Location only tentative.

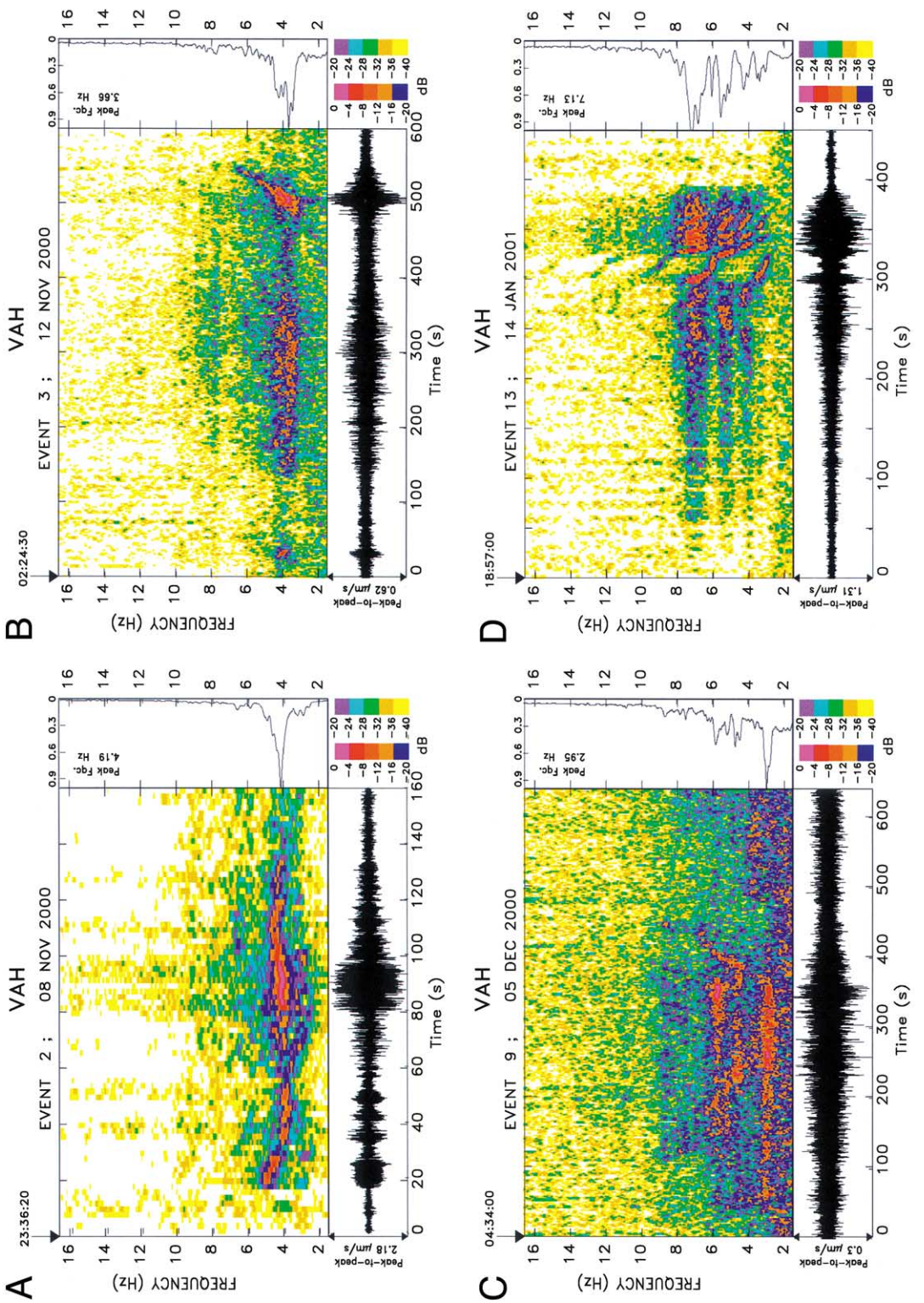
A
VAH
EVENT 2 ; 08 NOV 2000
23:36:20
Peak fqc. 4.19 Hz
Peak-to-peak 2.18 μm/s
FREQUENCY (Hz)
Time (s)
dB
B
VAH
EVENT 3 ; 12 NOV 2000
02:24:30
Peak fqc. 3.66 Hz
Peak-to-peak 0.62 μm/s
FREQUENCY (Hz)
Time (s)
dB
C
VAH
EVENT 9 ; 05 DEC 2000
04:34:00
Peak fqc. 2.95 Hz
Peak-to-peak 0.3 μm/s
FREQUENCY (Hz)
Time (s)
dB
D
VAH
EVENT 13 ; 14 JAN 2001
18:57:00
Peak fqc. 7.13 Hz
Peak-to-peak 1.31 μm/s
FREQUENCY (Hz)
Time (s)
dB

ally low level of the signals involved (at most a few μm/s at VAH), these observations stress, if need be, the importance of deploying T-phase stations on atolls (VAH) or on volcanic edifices fringed by coral reefs (RKT, RAR, TBI), whose steep slopes act to optimize the acoustic-to-seismic conversion [6].

3. Location

3.1. Location from hydroacoustic records

The principal events in the sequence were first located using the techniques developed during the Hollister swarm [4]: whenever possible, impulsive arrival times of sharp sub-events were used; in their absence, differential travel-times between stations were determined by cross-correlating the fluctuations with time of the frequency of monochromatic T waves. After implementing station corrections in order to compensate for the post-conversion land path traveled as a seismic wave at the receiver [6], the locations of the sources were inverted using the seasonally adjusted, laterally varying model of acoustic velocities of Levitus et al. [12]. The technique is enhanced by a Monte Carlo algorithm which injects Gaussian noise into the dataset of arrival times [13]; in the present study, we use a conservative standard deviation $\sigma_G = 4$ s, and iterate the process 500 times. A best-fitting ellipse is then computed for the resulting cluster of epicenters.

Representative results of this preliminary effort are shown in Fig. 3. In all cases, the epicenters locate in the general area of the Ross Sea, and of the Borchgrevink and George V coasts of Antarctica, but the limited azimuthal coverage provided by the band of available stations (at most 30°) results in weak resolution of epicentral distance. In general, we obtain meaningful constraints when the dataset includes the lateral stations RAR and RKT (e.g. Events 2 and 3; azimuth window: 27°); distance becomes exceedingly unconstrained when either one is unavailable (Events 12 and 13; azimuth window: 11–16°); and the location cannot converge in the absence of both RAR and RKT, the azimuthal window having then shrunk to no more than 2° (e.g. Event 1). Nevertheless, several statistically distinct groups can be identified, with Events 2 and 13 along the coasts, while the remaining epicenters locate in the center of the Ross Sea.

3.2. Seismic records at Antarctic stations

In view of these preliminary results, we conducted a systematic search for additional records of conventional seismic waves at Antarctic stations. We were able to identify signals at the IRIS station at Scott Base (SBA), at the GTSN station Vanda (VNDA), and at stations of the Mount Erebus Volcanic Observatory on Ross Island (MEVO; courtesy of Dr. Richard Aster). We were unable to detect any signal at the IRIS station at the South Pole (SPA), nor at the more distant stations Casey (CASY; IRIS) and Dumont d'Urville (DRV; Geoscope), along the coast of East Antarctica (Fig. 2A).

As shown in Fig. 4, the spectral characteristics of the Polynesian T phases and of the seismic phases at Antarctic stations often exhibit a spectacular similarity, leaving no possible doubt that they were generated by the same events. Major

←

Fig. 1. (A) T-phase record of Event 2 at Vaihoa. The figure is composed of three frames: The bottom one shows a 160-s time series of the ground velocity (in black), high-pass-filtered for $f \geq 2$ Hz. The frame at the right is a plot of the amplitude spectrum of the high-pass-filtered ground velocity record. The main color frame is a spectrogram representation of the distribution of spectral amplitude in the record, as a function of time and frequency. The color-coding is logarithmic, with the key (in dB relative to the most energetic pixel) given at bottom right. White pixels correspond to spectral amplitudes below −40 dB. Note the impulsive start of the signal and the slow, contained, fluctuation of the prominent frequency with time. (B) Same as (A) for Event 3. The time series is now 600 s long. Note the singular signal ending the sequence, featuring an increase of frequency with time. (C) Same as (A) for Event 9. Note the relative complexity of the spectrum and the trend towards an increase in frequency at the end of the main pulse (400 s into the signal). (D) Same as (A) for Event 13. Note the complex character of the spectrogram, especially in the final phases of the pulse, where the eigenfrequency tends to decrease with time ('gliding').

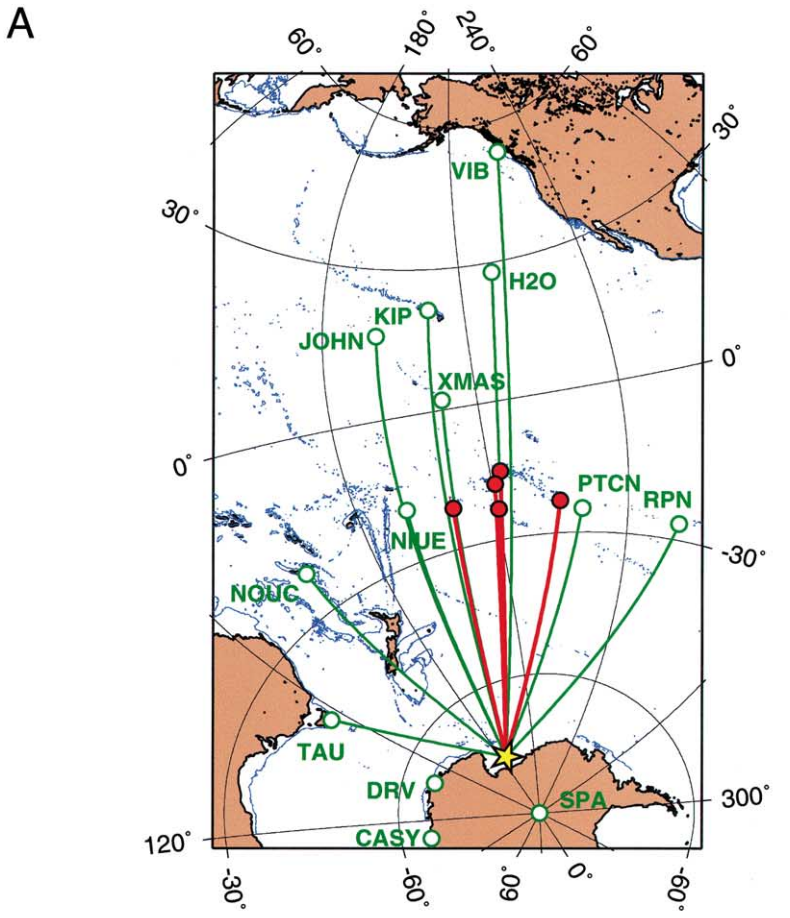
A
60°
180°
240°
60°
30°
30°
0°
0°
-30°
300°
120°
-30°
-60°
-90°
0°
-60°
VIB
H2O
KIP
JOHN
XMAS
PTCN
RPN
NIUE
NOUC
TAU
DRV
SPA
CASY

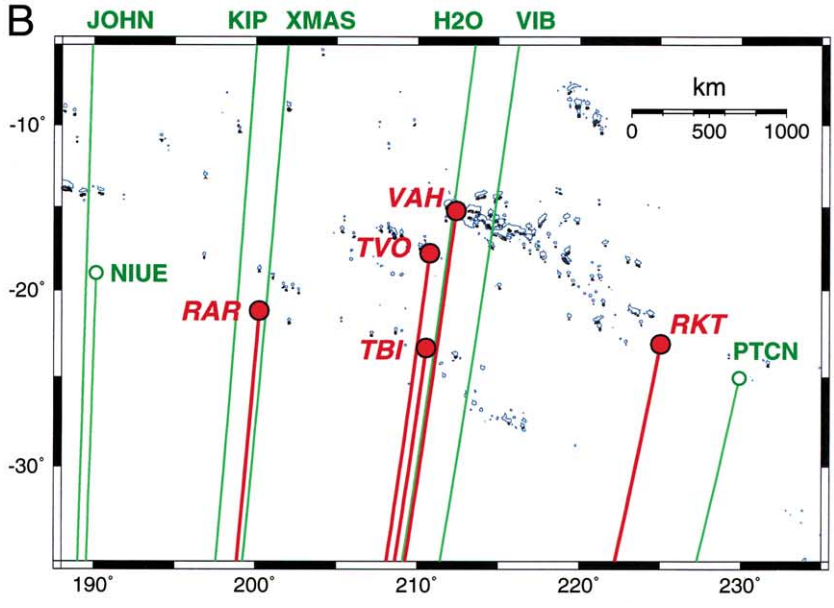
B
JOHN
KIP
XMAS
H2O
VIB
km
0
500
1000
-10°
-20°
-30°
VAH
TVO
NIUE
RAR
TBI
RKT
PTCN
190°
200°
210°
220°
230°

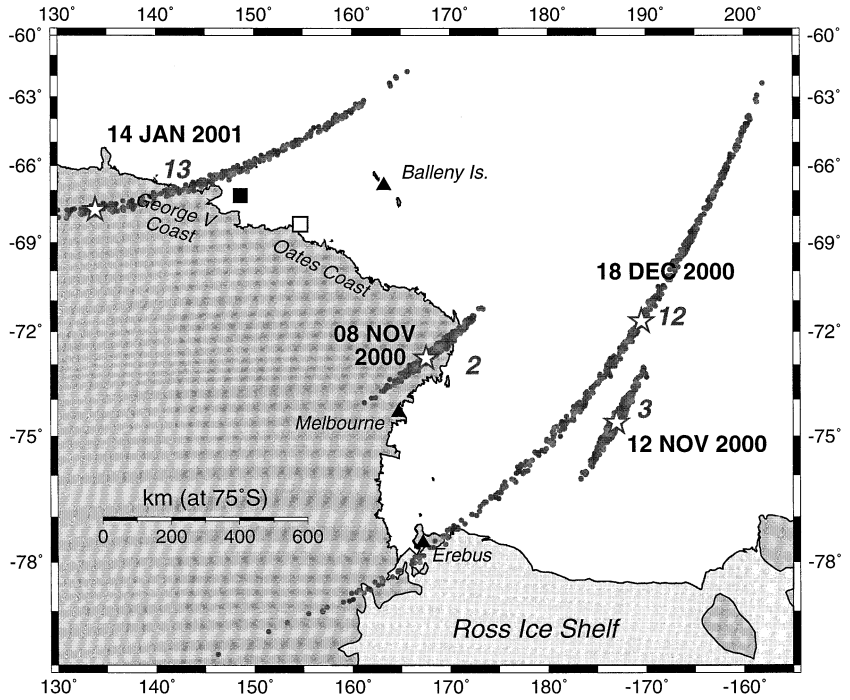

Fig. 3. Location of events 2, 3, 12 and 13 as constrained only by hydroacoustic data. The large open stars indicate the inverted epicenters and the individual dots the Monte Carlo clusters. The triangles show the locations of known volcanic (or fumarolic) activity, the solid square the presumed location of B-9B in early 2001, and the open one the last reported position of B-15B on 04 February 2002.

differences occur only, and occasionally, at the lower frequencies ($f < 2$ Hz), which simply expresses the high-pass filtering effect of the SOFAR channel and indicates that the waves recorded at the Antarctic stations are seismic, as opposed to hydroacoustic, in nature. As discussed below, their exact interpretation remains tentative.

In order to use the Antarctic seismic signals in a combined relocation with the Polynesian T phases, we need to know the velocity of seismic waves along the source-to-receiver path and hopefully to understand the nature of the relevant phases (P, S, interface...). For this purpose, we tested a series of relocations, for variable values of the velocity V to the Antarctic stations. In this experiment, we used a priori bounds of $V_{min} = 1.3$ km/s, thus including the possibility of an acoustic velocity in the Southern Sea, and $V_{max} = 8.25$ km/s, corresponding to a P_n velocity under the continental shelf, and we varied V in increments of 0.05 km/s. For each value of V, we quantify the quality of the relocation through the root mean squares (r.m.s.) of the residuals, σ. As shown in Fig. 5, a number of scenarios can occur.

←

Fig. 2. (A) Source and receiver map for the hydroacoustic waves used in this study. The map uses an oblique Mercator projection whose equator (vertical in the figure) is the great circle from the epicenter of Event 6 (star) to station TVO in Tahiti. Paths along which signals were detected (for at least one event) are shown in red, those for which no detection was made in green. The lone blue contour is at 1200 m and is used to assess the importance of blockage to the non-detecting stations (see text for details). A close-up of the Polynesian stations is shown in (B). (B) Close-up of (A) focusing on Polynesia, using the same color conventions, but this time a standard Mercator projection. Note that the path to VIB intersects the Tuamotu Plateau east of VAH, which may contribute to the absence of signal at VIB. To enhance clarity, additional stations on the island of Tahiti (and nearby Mehetia) are not shown; all are less than 75 km from TVO.

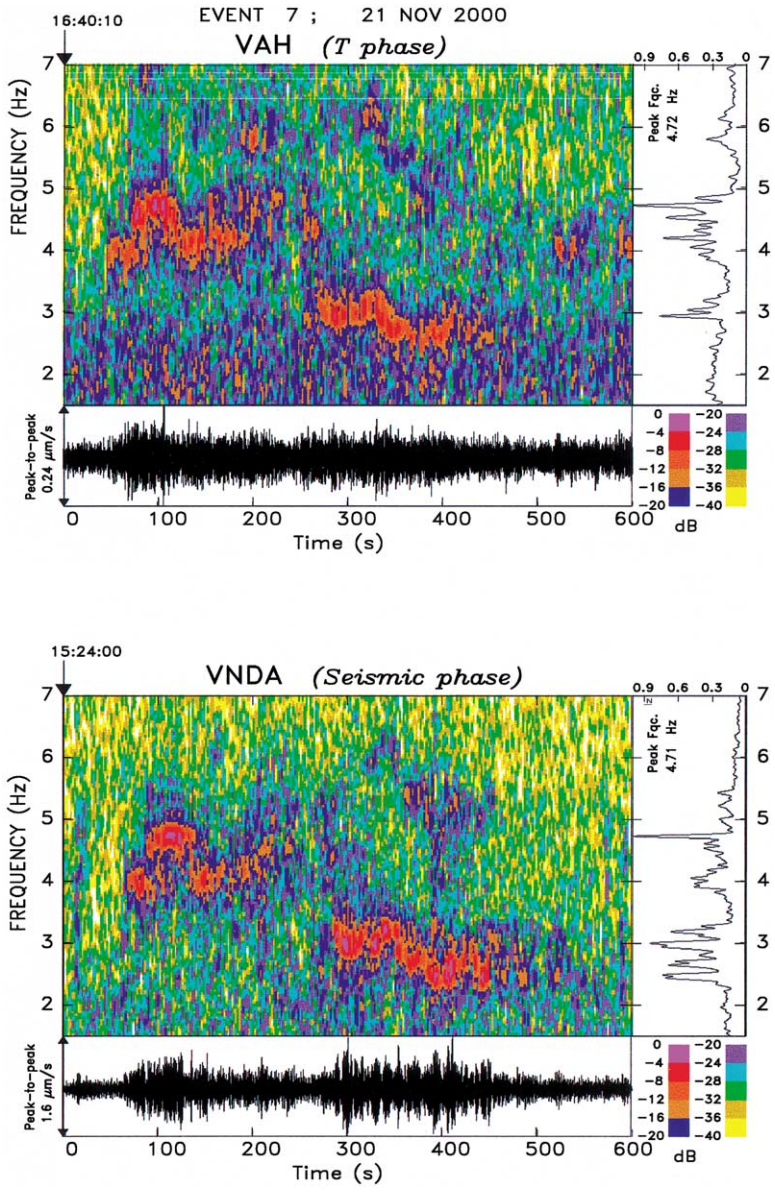

Fig. 4. Comparison of spectrograms from acoustic and seismic records from Event 7 at VAH (T phase; top) and at VNDA (seismic phase; bottom). Note the excellent correlation between the two spectra.

If only one station is available in Antarctica (Events 5, 8 and 9), V cannot be resolved, for it simply trades off with the position of the source along the major axis of the cluster of hydroacoustic locations. However, in the presence of several Antarctic seismic data (Events 3, 11 and 12), their *relative* times effectively resolve V and thus allow relocation with an acceptable σ, of generally less than 1.5 s. In all such cases, we can reject propagation as a conventional acoustic wave in water ($V \approx V_{\min}$) and in most cases, as a conventional P phase (either in the crust, $V \approx 6$ km/s, or as P_n

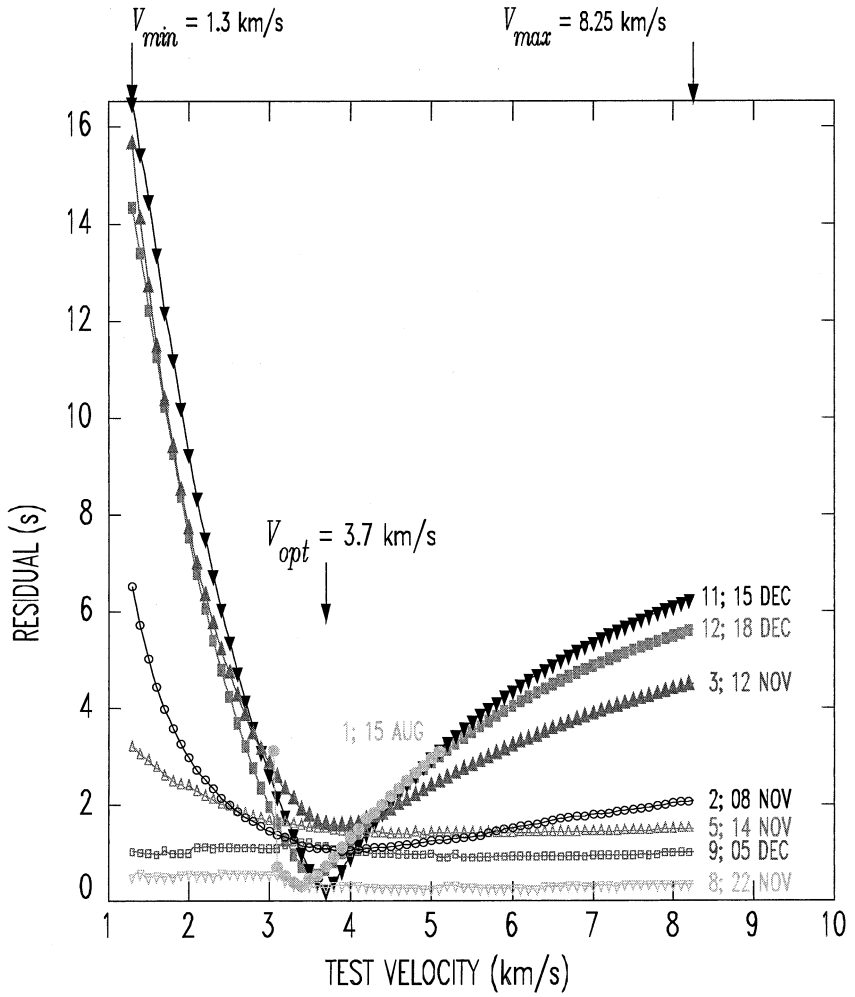

Fig. 5. Quality of combined seismic–hydroacoustic relocations for variable values of the seismic velocity V to the seismic receivers. For each event considered, we vary V from $V_{min} = 1.3$ to $V_{max} = 8.25$ km/s, and attempt to relocate the event. The open symbols correspond to events for which only one Antarctic station is available (VNDA). In the case of Event 1, the relocation fails for $V \geq 5.1$ km/s or $V \leq 3$ km/s.

under the Mohorovičić discontinuity, $V \approx V_{max}$). Rather, the best-fitting value V is in those cases $V_{opt} = 3.7 \pm 0.2$ km/s.

The only exception to this pattern is Event 2 (08 November 2000), for which Fig. 5 shows that σ remains acceptable (less than 2 s) even for $V = V_{max}$, although the best-fitting value is indeed $V = 3.9$ km/s, within the general range for the other events. This is because, in the particular geometry of Event 2, all possible T-phase epicenters (Fig. 3) are practically equidistant from VNDA and the SBA–MEVO group, which provides essentially no resolution of V.

The interpretation of V_{opt} is not straightforward and remains somewhat unresolved. On the one hand, it matches the velocity of P waves in recrystallized ice [14,15]. However, and even for Event 1, which may have occurred on the Ross Ice Shelf or at its boundary (see below), this interpretation is improbable, since the ice shelf is 300 m thick, i.e. less than 1/5 of the longest wavelengths recorded in Antarctica. For the other

events farther North, satellite imagery disproves the existence of a continuous layer of thick ice along the path to VNDA in the western part of the Ross Sea Basin (a shallow layer of sea ice, typically only a few meters thick, is totally transparent at the relevant frequencies).

Rather, we propose to interpret the arrivals at $V_{opt} = 3.7$ km/s as L_g wavetrains, generally interpreted as shear energy trapped in the continental crust (e.g. [16,17]).

As documented, for example by Bouchon [18] and Campillo et al. [19], L_g can be the first prominent arrival at regional distances in conditions where P arrivals do not emerge from noise, in particular for shallow crustal dislocation sources. Also, L_g energy can propagate efficiently at frequencies of a few Hz [18] and is distributed among the three components of ground motion, a property that we verified on a few available three-component records at VNDA. Furthermore, the value of V_{opt} falls in the range of predicted and observed L_g velocities at the relevant frequencies [20]. Finally, we will see that the epicentral locations of the Ross Sea events are on the continental shelf or at its boundaries, so that L_g wavetrains would not be blocked by transit over an oceanic path [21]. Note that we did not attempt to assign a magnitude m_{bLg} [22] to our events, given the singular character of their largely monochromatic spectra.

Despite our inability to identify the nature of the seismic phases recorded at Antarctic stations, we used the optimized velocity $V_{opt} = 3.7$ km/s for all seismic phases at Antarctic stations, to locate the Ross events from a combined dataset of acoustic and seismic arrival times.

3.3. Results

Out of the 13 sequences investigated, we obtain seven very well constrained locations, with semi-major axes of ≈ 25 km for the Monte Carlo ellipses (Events 2, 3, 5, 8, 10, 11 and 12), and two poorly resolved ones (Events 1 and 13). The remaining sequences (Events 4, 6, 7 and 9) are given tentative locations based on their temporal association with well located events. Fig. 6 shows that all epicenters, except Events 1, 2 and 13, fall in the center of the Ross Sea. The location of Event 13 (Fig. 1D), which was recorded neither by the Antarctic stations nor by RKT, could not be improved beyond the estimate obtained from Polynesian T phases (Fig. 3). Event 1 (15 August 2000) has a large uncertainty, but lies significantly South of the November–December group. As for Event 2 (08 November 2000), it has a well constrained epicenter just South of Cape Adare on the Borchgrevink Coast.

4. Discussion

4.1. Volcanism?

Because of our previous experience with the Hollister swarm [4], we first attempted to interpret the Ross signals as expressing volcanic activity. However, all nine located events cannot share a common epicenter. This is well documented by the Monte Carlo ellipses in Fig. 6, and was confirmed by a formal attempt at inverting the full dataset of arrival times for a common epicenter and distinct origin times. This resulted in unacceptable residuals of more than 1 min, even among Polynesian stations, and regardless of the value chosen for the Antarctic stations' velocity V, a result expected from the large separation between individual hydroacoustic Monte Carlo clusters (Fig. 3). We conclude that the source of the Ross Sea events moved with time in a SE to NW direction (with the exception of Event 2). Their spatio–temporal evolution is in sharp contrast with our previous experience of long-range hydroacoustic detection at volcanic sites such as Macdonald Seamount [23] and Hollister Ridge [4], and it strongly argues against a volcanic origin for the Ross Sea events.

To further eliminate this interpretation, we explored the quality of residuals when constraining the sources at either of the three known sites of volcanic (or fumarolic) activity in the area: Erebus (77.6°S; 167.2°E), Melbourne (74.35°S; 164.70°E) and the Balleny Islands (66°S; 163°E). In all cases tested, r.m.s. residuals exceeding several minutes made these locations unacceptable. In the case of Event 12, for example, Erebus

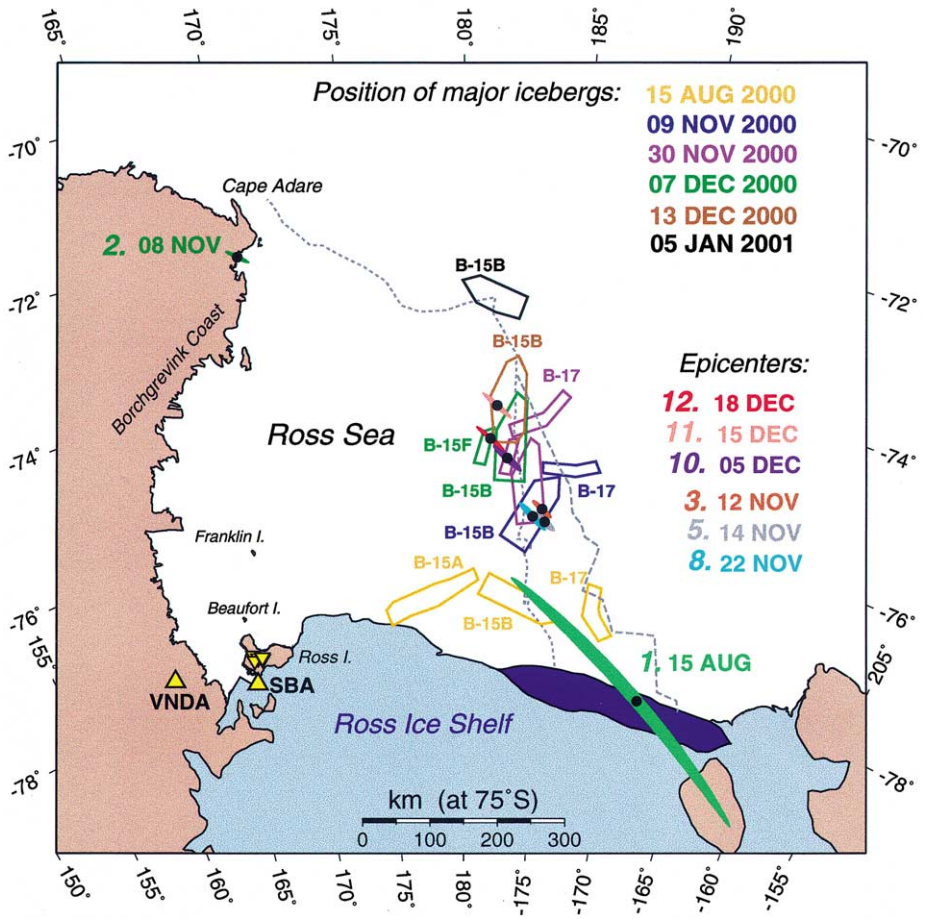

Fig. 6. Final epicenters obtained by joint inversion of T-phase and seismic data. The individual epicenters are shown as black solid dots and the associated Monte Carlo ellipses are shaded (see color key at right; Event numbers in italics). The position of B-15B is shown schematically at a number of dates from August 2000 to January 2001 (color-keyed; legend at top). Positions of the smaller iceberg B-17 are also shown at a few critical times until Late November 2000, when it breaks up into pieces following its collision with B-15B. The paths of the two icebergs are also shown continuously by the dotted (B-15B) and dashed (B-17) lines. The upward-pointing triangles show the global network seismic stations VNDA and SBA, the downward-pointing ones the MEVO network on Ross Island. The dark blue region schematizes the portion of the shelf which calved off and eventually gave rise to the B-15 and B-17 series. The projection is equidistant azimuthal centered at the South Pole.

was a legitimate epicenter on the basis of the RSP hydroacoustic data alone (Fig. 3), but the inclusion of the Antarctic dataset leads to a discrepancy of more than 9 min between Polynesian and Antarctic stations, this result being essentially independent of V because of the proximity of Erebus to SBA, MEVO, and to a large extent, VNDA. We reject volcanism as a source of the Ross Sea events, since even an uncharted volcanic source would have had to move hundreds of kilometers across the Ross Sea over a period of a few weeks.

4.2. Correlation with icebergs

We propose that the sources of the Ross Sea events lie within very large icebergs, documented to have calved off the Ross Ice Shelf in the (northern) Spring of 2000, and which were drifting across the Ross Sea in a NNW direction during

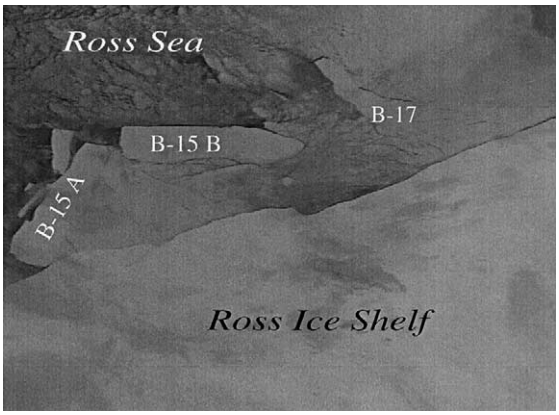

Fig. 7. Satellite image of B-15A and B-15B taken by the DMSP-F14 satellite on 10 August 2000 (courtesy of M. Lazzara). This view looks NNE from the Ross Ice Shelf into the Ross Sea. The total length of B-15B is 135 km. After [24].

the later part of the year. We base our interpretation on the dataset of reported coordinates and infrared satellite photographs available from the web site of the University of Wisconsin's Antarctic Meteorological Research Center [24].

Around March–April 2000, Iceberg B-15 (of truly gigantic proportions – 300 km by 40 km) and the smaller B-17 to the east calved off the shelf around 78°S, between 177 and 165°W. By 15 August 2000, the date of Event 1, B-15 had broken into two principal pieces, B-15A and B-15B, and several smaller ones (Fig. 7). Among those, B-15A then hugs the northern rim of the ice shelf, and eventually spends several months stuck between Ross, Beaufort and Franklin Islands, while the slightly smaller B-15B (still a massive unit at 135 km by 40 km) takes a northerly path towards the center of the Ross Sea, at an average drift velocity of 4 km/day (or 5 cm/s). Fig. 6 plots the positions of B-15B and B-17 at a number of dates between November 2000 and January 2001. During that time, B-15B engages in a large rotation, collides with B-17 in early November 2000, calves off a further small fragment, B-15F, on its west side, some time between 14 and 29 November 2000, and frees itself from B-17 as the latter breaks into pieces around 30 December 2000. By 05 January 2001, B-15B has taken a northwesterly direction, rounds Cape Adare about 03 May 2001 (it has then broken into two parts), and then progresses along the Oates Coast, where it currently (February 2002) lies around 155°E [25].

Fig. 6 shows a spectacular correlation between the epicenters of Events 3, 5, 8, 10, 11 and 12 (and hence presumably of the intervening Events 4, 6, 7 and 9) and the location of B-15B and B-17. In particular, the spatio–temporal evolution from the SSE group of epicenters (3, 5, 8) in November to the NNW one (10, 11, 12) in December mimics the drift and rotation of B-15B. In the case of the relatively poorly located Event 1 (on 15 August 2000), the northern end of its large Monte Carlo ellipse similarly intersects the position of B-15B on that same day.

We cannot propose any similarly compelling association with icebergs for the remaining Events 2 and 13. We note, however, that the relevant portions of the Borchgrevink and George V coasts feature numerous ice tongues, protruding into the ocean, and from which substantial icebergs calve off regularly. For example, in the case of Event 13 (poorly located on the basis of only a depleted set of hydroacoustic data), the cluster of Monte Carlo epicenters intersects the coast in the vicinity of the Mertz and Ninnis Glacier tongues, the latter (68°S; 148°E) having disintegrated in January 2000 through calving off two large (but not gigantic) icebergs. We have no information on the drift of these fragments after April 2000. Alternatively, we note the presence of the veteran, very large iceberg B-9B (2900 km^2), which was stationary at 67.2°S; 148.6°E (solid square in Fig. 3) between 06 November 2000 and 26 January 2001. Given the poor quality of Event 13's location, we cannot rule out that its source was B-9B.

We could find no information on possible icebergs in the vicinity of Epicenter 2 (08 November 2000); we note, however, its proximity to the mouth of Tucker Glacier in Borchgrevink Coast.

4.3. Possible triggering mechanisms

We focus henceforth on the remarkable cluster of events (1, 3–12) which correlate with the position of B-15B as it drifts northwards across the Ross Sea. As discussed below, we can offer only

vague speculation as to the nature of the events taking place inside the icebergs and generating the hydroacoustic and seismic signals studied. Whatever these phenomena may be, it is remarkable that they take place only during a small part of the long drift of B-15B from the Ross Ice Shelf to Cape Adare and beyond, namely during a 36-day window and over a distance of less than 200 km (with the exception of Event 1, farther south). In particular, B-15B becomes silent after 18 December 2000, and during its 4-month voyage to Cape Adare. We know of no prominent bathymetric feature which would explain this pattern through hydroacoustic blockage along the path to Polynesia. Rather, B-15B's silence must reflect the cessation of the physical source process.

Possible mechanisms for the excitation of an oscillator that would be geographically (or temporally) controlled include collisions with other ice masses and rubbing on the sea floor. We note in particular that the activity in B-15B starts on 12 November 2000, a time when it has collided with the more easterly B-17, and ceases after 18 December 2000. A possible scenario would then correlate the Ross Sea events with the collision between B-15B and B-17, which lasted at least 1 month, until B-17 broke into pieces at the end of December. Another scenario would invoke friction on the floor of the Ross Sea, as a mechanism controlling the mechanical sources in the icebergs. Bathymetric coverage of the Ross Sea is scarce, especially since the relevant area lies outside the southern limit (72°S) of the satellite altimetry database [26]. However, the northern portion of B-15B's path (traveled westwards after 01 January 2001) most probably lies over deep water, whereas its southern portion (traveled northwards) is over the continental shelf. We can only speculate as to the presence of large seamounts or other underwater structures, against which the iceberg could have rubbed, but the spatio–temporal distribution of the Ross Sea events would be in very general agreement with this scenario. We also note that significant iceberg furrows have been documented on the sea floor, including around Antarctica, at depths as great as 400–500 m [27,28], making it legitimate to assume that motion over the continental shelf at similar depths would occasionally involve scraping against bathymetric features. Finally, as shown by Campillo et al. [19], a superficial source (such as an iceberg scraping the ocean floor) will excite L_g most efficiently, whereas the excitation of P_g would be relatively insensitive to depth; these properties would lead naturally to L_g being the prominent seismic phase for sources exciting the solid Earth at the water–crust interface.

4.4. Speculation about the possible nature of the resonators

Regarding the physical nature of the sources of the Ross Sea signals, the pre-eminence of distinctive frequencies (typically 4 Hz) in many spectra (occasionally with harmonics) suggests the oscillation of a resonator. In this respect, our sources differ significantly from the 'icequakes' widely observed at seismic stations deployed on ice. The latter correspond to the failure of cracks in the ice, under stresses induced either thermally or by the slow flow of the ice [29]. Being essentially instantaneous sources, they are characterized by short durations and a broad spectrum featuring high frequencies [30]. Even the so-called 'low-frequency icequakes', attributed to calving off ice blocks from glaciers [31] and occasionally featuring a monochromatic spectrum [32], are of much shorter duration than the Ross events.

To investigate more in detail the spectral characteristics (eigenfrequency and quality factor Q) of a representative signal, we selected the VAH record from Event 4 (on 12 November 2000) because of its exceptional duration (3 h). We use a running window of 81.9 s duration (4096 samples), offset 10 s at a time. At each step, we then identify the frequency f_0 at which the spectral amplitude $X(f)$ reaches its maximum, which we interpret as the eigenfrequency of the resonator, and we fit a resonance curve of the form:

$$X_r(f) = \frac{A}{\sqrt{(f-f_0)^2 + \dfrac{\pi^2 f_0^2}{Q^2}}} \quad (1)$$

to the shape of the spectral amplitude $X(f)$ in the frequency interval I $\{f_0-0.125\ \text{Hz} \le f \le f_0+0.125$

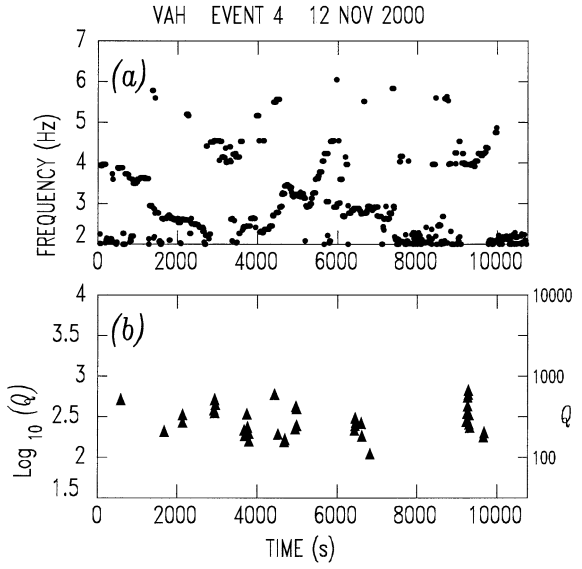

Fig. 8. Evolution of spectral properties with time during Event 4. (a) Frequency f_0 at maximum of spectral amplitude. (b) Values of Q retained by application of the thresholds discussed in text.

Hz}. We keep track of the amplitude $X(f_0)$ of the spectral peak, and of the quality of fit $QUAL$ of the resonance curve (1) to the observed spectral line, which we define as the inverse of the r.m.s. residual σ between $X(f)$ and $X_r(f)$ over the interval I, scaled by the maximum spectral amplitude: $QUAL = X(f_0)/\sigma$. We retain only values of Q for those windows where $X(f_0)$ is at least 40% of its maximum value and for which the parameter $QUAL$ is at least 10, which leaves a total of 41 Q values. The two frames in Fig. 8 show the variation of f_0 and Q as a function of time t, taken at the center of the running window.

While f_0 can remain remarkably constant over intervals of time of a few minutes (see Fig. 1), Fig. 8a shows that it varies significantly on a time scale of tens of minutes. Changes in f_0 can be continuous (e.g. the 'gliding' observed at the start of the record), or sharp and stepwise, the windows with stronger and cleaner signals being more stable in frequency. This would require the presence of several oscillators, some of them capable of an evolution with time of their eigenfrequency, which in turn most probably expresses an evolution of their dimension.

The quality factors Q of the resonators range between 100 and 650, with an inverse average value of 250. This value is much greater than typically reported for the sources of volcanic tremor ($Q = 5$–10; [33]) or even during the Hollister swarms ($Q = 20$–50; [4]), which constitutes an additional strong argument against a volcanic origin for the Ross Sea signals. The attenuation of seismic waves in ice was studied in the Greenland icefield by Langleben [34], who reported a fall-off coefficient $c_1 = 4.45 \times 10^{-2}$ dB m^{-1} kHz^{-1}, equivalent to $Q = 166$, and in sea ice by Kohnen [35], who gives a slope of attenuation with frequency $q = 0.56 \times 10^{-5}$ m^{-1} Hz^{-1}, equivalent to $Q = 175$. Note, however, that these values were measured at considerably higher frequencies in both studies and on longitudinal waves in the latter.

Speculating further on the possible physical nature of the resonator, we note the approximate dimensions of B-15B: 135 km by 40 km, and we take its thickness as at least 300 m, based on an estimation of the emerged fraction from airborne photographs [24], and of the thickness of the Ross Ice Shelf from seismic soundings [15]. We can then eliminate gravitational oscillations as the source of the signals, since the bobbing frequency of the iceberg on the sea would be on the order of 30 mHz (conversely, the observed frequency of 4 Hz would correspond to a thickness of only 1.7 cm); rolling and pitching eigenfrequencies would also be much lower than observed – on the order of 20 mHz.

Rather, the frequencies observed could represent various eigenmodes of oscillation of the iceberg. For example, in the case of a 300-m thick ice layer, the eigenfrequency of a vertical shear mode would be 3.07 Hz (using a shear velocity $\beta = 1.84$ km/s, corresponding to a Poisson ratio of 0.34). The eigenfrequency of a fundamental 'Crary' mode [36,37] (essentially a shear wave propagating horizontally with a phase velocity equal to the P velocity α) would be 3.51 Hz for the ice sheet in a vacuum; it could be affected by the presence of water [37], but its order of magnitude would remain in general agreement with the resonance frequencies observed in our signals. This interpretation would be particularly likely under the assumption that the ice mass is set in resonance by scraping the ocean floor, or rubbing against

another ice mass; it could also explain the presence of harmonics, since several modes would be excited by a source essentially similar to hitting a bell, and resulting in musical 'richness'. However, under this scenario, the iceberg would resonate at a set of discrete, well defined pitches, and the observed continuous fluctuation of eigenfrequency with time would be difficult to explain.

Another scenario would involve the resonance of a fluid-filled cavity in a mode comparable to the oscillation of magma within a fissure in a volcanic system [33], the eigenfrequencies of such as a resonator being complex functions of its size and shape, and of the impedance contrast between the fluid filling the crack and the surrounding medium [8]. In the case of icebergs, the fluid would have to be water, but the almost certain presence of air bubbles could greatly reduce its sound speed, making 'resonance at long period [...] possible in a short crack' [8]. By analogy with models for volcanic tremor, it is estimated that cracks of dekametric size may justify the range of observed frequencies – typically from 2 to 7 Hz for the fundamental [8]. Furthermore, this scenario would explain the observed fluctuations of frequency with time, as both the dimension of the resonator and the supply of air bubbles could be expected to vary with time continuously, for example during filling or emptying of the fluid in the crack. A catastrophic runaway failure of the crack may explain the final stages of evolution observed in Fig. 1B (when the crack may shrink and eventually close), or Fig. 1D (if the crack opens fully and potentially an ice chunk separates). These interpretations remain of course highly speculative at this point.

5. Conclusions

We have documented prolonged episodes of hydroacoustic activity in the Ross Sea during the months of August–December 2000. By combining datasets of T phases recorded in Polynesia with regional seismic phases recorded at Antarctic stations, we obtain epicentral locations correlating systematically with the position of large icebergs, specifically B-15B and B-17, which were drifting in the Ross Sea at that time, and thus we conclude that the signals originated at or inside the icebergs. Despite a broad variability in the spectral characteristics of the Ross events, they cannot be compared to seismic sources previously identified and analyzed in the ice environment, such as icequakes and calving events. Rather, our observations define a new kind of source capable of contributing hydroacoustic energy to the SOFAR channel over extended periods of time. The presence of preferential frequencies in the 3–7 Hz range (often associated with overtones) clearly implicates the resonance of an oscillator, whose exact nature presently eludes us. In the context of the use of hydroacoustic waves for monitoring of the CTBT, it is clear that a deeper investigation of the phenomena involved is warranted; a possible avenue would involve the direct deployment of portable seismic stations on massive icebergs known to be calving off the major Antarctic ice shelves, most recently C-19 in May 2002 [24].

Acknowledgements

We thank Rick Aster for providing the Erebus network data, Bernard Chouet, Michel Bouchon and Michel Vallon for discussion, and Jackie Caplan-Aucherbach and another reviewer for helpful comments. Matthew Lazzara kindly provided a customized version of Fig. 7. Maps were drawn using the GMT software of Wessel and Smith [38]. This research was supported at Northwestern University by the Department of Defense under Contract DTRA01-C-0065.

References

[1] E.A. Okal, J. Talandier, K.A. Sverdrup, T.H. Jordan, Seismicity and tectonic stress in the Southcentral Pacific, J. Geophys. Res. 85 (1980) 6479–6495.
[2] J. Talandier, G.T. Kuster, Seismicity and submarine volcanic activity in French Polynesia, J. Geophys. Res. 81 (1976) 936–948.
[3] E.A. Okal, T-phase stations for the International Monitoring System of the Comprehensive Nuclear-Test Ban Treaty: A global perspective, Seismol. Res. Lett. 72 (2001) 186–196.
[4] J. Talandier, E.A. Okal, Monochromatic T waves from

underwater volcanoes in the Pacific Ocean: Ringing witnesses to geyser processes?, Bull. Seismol. Soc. Am. 86 (1996) 1529–1544.
[5] L. Géli, D. Aslanian, J.-L. Olivet, I. Vlastelić, L. Dosso, H. Guillou, H. Bougault, Location of Louisville hotspot and origin of Hollister Ridge: Geophysical constraints, Earth Planet. Sci. Lett. 164 (1998) 31–40.
[6] J. Talandier, E.A. Okal, On the mechanism of conversion of seismic waves to and from T waves in the vicinity of island shores, Bull. Seismol. Soc. Am. 88 (1998) 621–632.
[7] M.T. Hagerty, S.Y. Schwartz, M.A. Garcés, M. Protti, Analysis of seismic and acoustic observations at Arenal Volcano, Costa Rica, 1995–1997, J. Volcan. Geotherm. Res. 101 (2000) 27–65.
[8] B. Chouet, New methods and future trends in seismological volcano monitoring, in: R. Scarpa, R.I. Tilling (Eds.), Monitoring and Mitigation of Volcano Hazards, Springer, Berlin, 1996, pp. 23–97.
[9] E.A. Okal, J. Talandier, T waves from the great 1994 Bolivian deep earthquake in relation to channeling of *S* wave energy up the slab, J. Geophys. Res. 102 (1997) 27421–27437.
[10] E.A. Okal, P.-J. Alasset, O. Hyvernaud, F. Schindelé, The deficient T waves of tsunami earthquakes, Geophys. J. Int., in press.
[11] D. Reymond, O. Hyvernaud, J. Talandier, E.A. Okal, T-wave detection of two underwater explosions off Hawaii on April 13, 2000, Bull. Seismol. Soc. Am., submitted.
[12] S. Levitus, T.P. Boyer, J. Antonov, R. Burgett, M.E. Conkright, World Ocean Atlas 1994, NOAA/NESDIS, Silver Springs, MD, 1994.
[13] M.E. Wysession, E.A. Okal, K.L. Miller, Intraplate seismicity of the Pacific Basin, 1913–1988, Pure Appl. Geophys. 135 (1991) 261–359.
[14] E. Thiel, N.A. Ostenso, Seismic studies on Antarctic ice shelves, Geophysics 26 (1961) 706–715.
[15] B.C. Beaudoin, U.S. ten Brink, T.A. Stern, Characteristics and processing of seismic data collected on thick, floating ice: Results from the Ross Ice Shelf, Antarctica, Geophysics 57 (1992) 1359–1372.
[16] F. Press, M. Ewing, Two slow surface waves across North America, Bull. Seismol. Soc. Am. 42 (1952) 219–228.
[17] L. Knopoff, Interpretation of L_g, Geophys. J. Roy. Astron. Soc. 33 (1973) 387–402.
[18] M. Bouchon, The complete synthesis of seismic crustal phases at regional distances, J. Geophys. Res. 87 (1982) 1735–1741.
[19] M. Campillo, M. Bouchon, B. Massinon, Theoretical study of the excitation, spectral characteristics, and geometrical attenuation of regional seismic phases, Bull. Seismol. Soc. Am. 74 (1984) 79–90.
[20] M. Cara, J.B. Minster, Multi-mode analysis of Rayleigh-type L_g, Bull. Seismol. Soc. Am. 71 (1981) 973–984.
[21] L. Knopoff, R.G. Mitchel, E.G. Kausel, F. Schwab, A search for the oceanic L_g phase, Geophys. J. Roy. Astron. Soc. 56 (1979) 211–218.
[22] O.W. Nuttli, Seismic wave attenuation and magnitude relation for Eastern North America, J. Geophys. Res. 78 (1973) 876–885.
[23] J. Talandier, E.A. Okal, Crises sismiques au volcan Macdonald (Océan Pacifique Sud), C.R. Acad. Sci. Paris Sér. II 295 (1982) 195–200.
[24] Antarctic Meteorological Research Center, http://amrc.ssec.wisc.edu, Univ. Wisconsin, Madison, WI, 2002.
[25] National Ocean and Atmospheric Administration, http://www.noaanews.noaa.gov/stories/s862.htm, U.S. Dept. of Commerce, 2002.
[26] W.H.F. Smith, D.T. Sandwell, Bathymetric prediction from dense satellite altimetry and sparse shipboard bathymetry, J. Geophys. Res. 99 (1994) 21803–21824.
[27] I.McK. Harris, P.G. Jollymore, Iceberg furrow marks on the continental shelf Northeast of Belle Isle, Newfoundland, Can. J. Earth Sci. 11 (1974) 443–452.
[28] P.W. Barnes, R. Lien, Icebergs rework shelf sediments to 500 m off Antarctica, Geology 16 (1988) 1130–1133.
[29] K.G. Neave, J.C. Savage, Icequakes on the Athabasca glacier, J. Geophys. Res. 75 (1970) 1351–1362.
[30] C. Sinadinovski, K. Muirhead, S. Spiliopoulos, D. Jespen, Effective discrimination of icequakes on seismic records from Mawson station, Phys. Earth Planet. Inter. 113 (1999) 203–211.
[31] A. Qamar, Calving: A source of low-frequency seismic signals from Columbia Glacier, Alaska, J. Geophys. Res. 93 (1988) 6615–6623.
[32] D. VanWormer, E. Berg, Seismic evidence for glacier motion, J. Glaciol. 12 (1973) 259–265.
[33] K. Aki, M. Fehler, S. Das, Source mechanism of volcanic tremor; fluid-driven crack models and their application to the 1963 Kilauea eruption, J. Volcanol. Geotherm. Res. 2 (1977) 259–287.
[34] M.P. Langleben, Attenuation of sound in sea ice, 10–500 kHz, J. Glaciol. 8 (1969) 399–406.
[35] H. Kohnen, Über die Absorption elastischer longitudinaler Wellen im Eis, Polarforschung 39 (1970) 269–275.
[36] M. Ewing, A.P. Crary, Propagation of elastic waves in ice, II, Physics 5 (1934) 181–184.
[37] F. Press, M. Ewing, Propagation of elastic waves in a floating ice sheet, Trans. AGU 32 (1951) 673–678.
[38] P. Wessel, W.H.F. Smith, Free software helps map and display data, EOS Trans. AGU 72 (1991) 441 and 445–446.